3D synthetic aperture and steering for controlled-source electromagnetics

Allison Knaak and Roel Snieder, Colorado School of Mines
Yuanzhong Fan and David Ramirez-Mejia, Shell International Exploration and Production

Controlled-source electromagnetics (CSEM) is a geophysical electromagnetic method used to detect hydrocarbon reservoirs in marine settings. Used mainly as a derisking tool by the industry, the applicability of CSEM is limited by the size of the target, low-spatial resolution, and depth of the reservoir. Synthetic aperture, a technique that increases the size of the source by combining multiple individual sources, has been applied to CSEM fields to increase the detectability of hydrocarbon reservoirs. We apply synthetic aperture to a 3D synthetic CSEM field with a 2D source distribution to evaluate the benefits of the technique. The 2D source allows steering in the inline and crossline directions. We present an optimized beamforming of the 2D source which increases the detectability of the reservoir. With only a portion of three towlines spaced 2 km apart, we enhance the anomaly from the target by 80%. We also demonstrate the benefits of using the Poynting vector to view CSEM fields in 3D. Synthetic aperture, beamforming, and Poynting vectors are tools that will increase the amount of information gained from CSEM survey data.

Introduction

Controlled-source electromagnetics (CSEM) is a geophysical electromagnetic method used for detecting hydrocarbon reservoirs in marine settings. First developed in academia in the 1970s, a CSEM survey involves towing a horizontal antenna just above the seafloor, where electromagnetic receivers are placed. The oil industry has used CSEM for almost two decades as a derisking tool in the exploration of hydrocarbon reservoirs (Constable and Srnka, 2007; Edwards, 2005; Constable, 2010). CSEM is often used in conjunction with other geophysical methods such as seismic but it has limitations that prevent it from gaining more widespread use in industry. The limitations come from the fact that the electromagnetic field in CSEM is a predominantly diffusive field. For the reservoir to be detectable, the lateral extent of the reservoir must be large enough compared to the depth of burial, and enough of the weak signal from the reservoir must reach the receivers (Constable and Srnka 2007; Fan et al., 2010). Also compared to seismic methods, the spatial resolution of CSEM is low (Constable, 2010).

These drawbacks prompted an investigation of how to improve the signal received from the reservoir through synthetic aperture, a method developed for radar and sonar that constructs a larger virtual source by using the interference of fields created by different sources (Barber, 1985; Bellettini and Pinto, 2002). Fan et al. (2010) demonstrate for a 1D array of sources that the wave-based concept of synthetic aperture sources can also be applied to CSEM fields and that it can be used to improve the detectability of reservoirs. The similarities in the frequency-domain expressions of diffusive and wavefields show that a diffusive field at a single frequency does have a specific direction of propagation. Synthetic aperture allows the use of beamforming, a technique used to create a directional transmission from a source or sensor array (VanVeen and Buckley, 1988). One can apply the basic principles of phase shifts and addition to electromagnetic fields to change the direction in which the energy moves. The shifts create constructive and destructive interference between the energy propagating in the field which, with a CSEM field, can increase the illumination of the reservoir (Fan et al., 2012). Manipulating diffusive fields by using interference is not necessarily new; physicists have previously used the interference of diffusive fields for a variety of applications (Yodh and Chance, 1995; Wang and Mandelis, 1999). Fan et al. (2010) applied the concepts of synthetic aperture and beamforming to CSEM fields with one line of sources. They demonstrated the advantages of synthetic aperture steering and focusing to CSEM fields; the main improvement is to the detectability of targets shallower and deeper than the typical range of depths for CSEM.

In this article, we introduce the concept of 3D synthetic aperture for electromagnetic fields; the source distribution is expanded from sources along a line to 2D with multiple parallel lines allowing the fields to be steered in 3D. We also briefly discuss a visualization tool to view 3D electromagnetic fields.

Mathematical basis

Fan et al. (2010) first applied synthetic aperture to controlled-source electromagnetic fields with one line of sources. Synthetic aperture was used earlier for radar, sonar, medical imaging, and other applications (Barber, 1985; Bellettini and Pinto, 2002; Jensen et al., 2006). One reason synthetic aperture, a wave-based concept, was not originally applied to CSEM fields is that it was widely assumed diffusive fields could not be steered because they have no direction of propagation (Mandelis, 2000). Løseth et al. (2006) found that electromagnetic fields can be described in both diffusion- and wave-equation terms. The similarities in these approaches show the 3D scalar diffusion equation has a plane wave solution at a single frequency with a defined direction of propagation which allows the direction of the field to be manipulated by synthetic aperture (Fan et al., 2010). The equation for synthetic aperture is given by

$$S(\mathbf{r},\omega) = \iint_{sources} e^{-A(\mathbf{s})} e^{-i\Delta\Psi(\mathbf{s})} F(\mathbf{r},\mathbf{s},\omega) d\mathbf{s}\,, \qquad (1)$$

where, for each source $\mathbf{s}$, $\Delta\Psi$ is a phase shift and A is an energy compensation coefficient. $F(\mathbf{r}, \mathbf{s}, \omega)$ is a general field; it could be any component the electric or magnetic field at receiver $\mathbf{r}$ and source $\mathbf{s}$. For a plane wave synthetic aperture

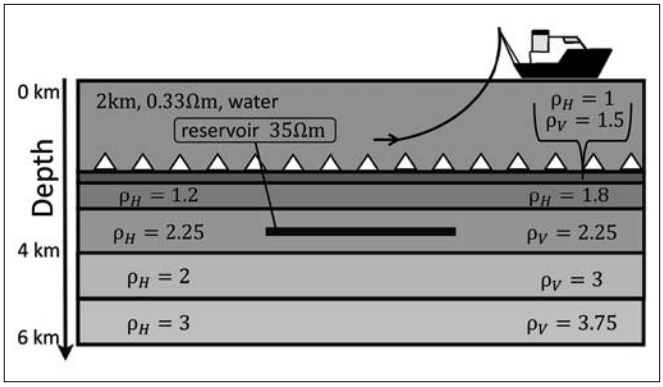

Figure 1. *The model used to create the synthetic CSEM data. The values of ρ_H and ρ_V are the resistivity of the layer in the horizontal and vertical directions, respectively, given in ohm-meters.*

source, the field is steered by applying a phase shift and energy compensation terms defined by

$$\Delta\Psi(\mathbf{s}) = k(\hat{\mathbf{n}} \cdot \mathbf{\Delta s}) \tag{2}$$

$$\hat{\mathbf{n}} = \begin{pmatrix} \cos\varphi \sin\theta \\ \sin\varphi \sin\theta \\ \cos\theta \end{pmatrix} \tag{3}$$

$$A(\mathbf{s}) = k(\mathbf{\Delta s} \cdot \mathbf{a}) \tag{4}$$

The shift $\Delta\Psi(\mathbf{s})$ is a function of the wavenumber, the steering angle $\hat{\mathbf{n}}$, and a location vector $\mathbf{\Delta s}$. The unit vector $\hat{\mathbf{n}}$ in Equation 3 defines the steering direction of the phase shift which is controlled by angles θ and φ. The dip of the direction of the steering angle, represented by θ, is measured with respect to the vertical. The angle φ represents the azimuthal direction. The quantity $\mathbf{\Delta s}=\mathbf{s}_n-\mathbf{s}_1$ is the relative location of an individual source $\mathbf{s}_n$ and the source defined to be at the bottom left corner of the survey footprint $\mathbf{s}_1$. The energy-compensation term $A(\mathbf{s})$ in Equation 4 is the dot product of the distances in $\mathbf{\Delta s}$ and the vector $\mathbf{a}$ which is composed of $[a_i \;\; a_c \;\; a_d]$. These three values define the weighting components for the inline direction, crossline direction, and depth, respectively.

In a traditional CSEM survey, a source is towed along parallel lines (inline direction) over receivers on the seafloor; the source and receiver geometry in the examples in this article follow the traditional design. The exponential weighting (Equation 4) equalizes the amplitudes and creates interference needed to steer diffusive fields; other methods of weighting exist (Fan et al., 2012). For a homogeneous medium, the phase shift and energy-compensation terms are set to be equal because the decay of the field is proportional to the phase shift, and the attenuation coefficient in Equation 1 is equal to the wave number (Fan et al., 2011). For a realistic CSEM field, the background is heterogeneous and the phase shift and energy-compensation terms are not equal. In this case, the energy compensation term accounts for the diffusive loss, decreases the background field to create a window to view the secondary field and equalizes the interfering fields to create destructive interference (Fan et al., 2011, 2012).

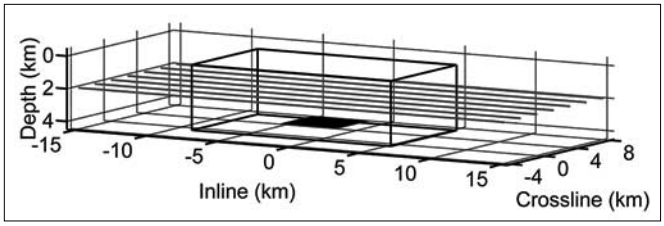

Figure 2. *The geometry of the CSEM survey for the synthetic data. The seven towlines are shown as black lines. The reservoir is the black rectangle. The coverage of the sampling points of the electromagnetic field is outlined by the 3D box.*

The proper choice for the energy-compensation term and the phase shift for a CSEM field are determined by maximizing a quantity of the CSEM field that indicates the presence of a reservoir. For this article, we choose to use the ratio of the absolute value of the inline component of the electric field with and without the reservoir; we call this value the detectability ratio. This measure is commonly used in industry to quantify the anomaly from hydrocarbon reservoirs (Constable and Srnka, 2007). In future research, we will investigate other types of metrics for the quality of the synthetic aperture source. The optimization of the steering parameters of the synthetic aperture source finds the values of four parameters: θ, φ, a_i, and a_c that control the steering. The a_d component of the weighting term is not included because the depth component of $\mathbf{\Delta s}$ is zero for this survey; if sources in a survey are at different depth then this term becomes relevant. We selected a range for each variable and combinations of the parameters were put into the steering equation until the combination was found that produced the maximum average detectability ratio between the inline component of the electric field with a reservoir and the field without a reservoir. The outcome from the steering and optimization is discussed in the next section.

Numerical examples

We use synthetic controlled-source electromagnetic fields to demonstrate the benefits of steering with 3D synthetic aperture. We computed a synthetic data set using a code from the CEMI group at the University of Utah (Hursán and Zhdanov, 2002). The synthetic data contain all three components of both the electric and magnetic fields. The model contains seven towlines 2 km apart and 15 km long over a 4 km × 4 km × 50 m reservoir at a depth of 3.5 km. All parameters are within the ranges for a typical CSEM survey. The source is a 300-m horizontal dipole with a frequency of 0.2 Hz. The resistivity of the Earth model varies with depth and direction; the model is shown in Figure 1. The reservoir has a resistance of 35 Ωm. Because of the large water depth (2 km), the air wave is weak at the acquisition level (sea bottom). The fields are sampled at points on the seafloor and at several depths in the subsurface. The

sampling points in the subsurface give information about the flow of energy around and near the reservoir. The points span –7 km to 7 km in the inline direction and –4 km to 4 km in the crossline direction (spaced every 250 m). In depth, the sample points range from 0 km to 4 km and occur at a sampling interval of 200 m. Figure 2 displays the survey geometry.

We create a 2D synthetic aperture source to demonstrate inline and crossline steering. The source extends from –6.6 km to –1.8 km in the inline direction and is 4 km wide in the crossline direction. The individual sources are sparsely spaced in the crossline direction, 2 km apart, and more densely spaced in the inline direction, 300 m apart. The choice of location of the 2D source region is offset from the reservoir to test the strength of the inline and crossline steering. The optimization discussed above finds the optimum steering angles θ and φ and two components of the energy compensation terms a_i and a_c. For these examples, the range of the steering angles θ and φ is from zero to $\pi/2$. The range for the energy compensation terms, a_i and a_c is zero to one. The increase in the detectability of the reservoir needs to occur over an area, not just a single point, to ensure the signal is recorded by a receiver placed in the region of interest. We include this spatial requirement by defining an area where we would expect to find the anomaly from the reservoir. We use the detectability ratio of a single source in the middle of our proposed 2D source to determine the area of expected increased anomaly. Then, the detectability ratio in the defined area is averaged and the maximum average detectability ratio defines the best steering. We defined the area of expected increased anomaly to be 0 km to 4 km in the inline and crossline direction for this synthetic model (the dashed box in Figure 3). The maximum average detectability ratio in that area results in these values for the specified 2D source: $\theta = 64°$, $\varphi = 83°$, $a_i = 0.125$, $a_c = 0.875$. The steering angles are reasonable for the geometry of the source relative to the reservoir in that the steered source sends the energy down and toward the reservoir. Figure 3 depicts the detectability ratio of the inline electric field with and without the reservoir at the seafloor for a single source (Figure 3a), an unsteered 2D synthetic aperture source (Figure 3b), and a steered 2D synthetic aperture source (Figure 3c). The average detectability ratio between the field with and without the reservoir for a single source (at –4.5 km in the inline direction and –2 km in the crossline direction) in the area we expect the anomaly is 1.11, meaning there is a 11% anomaly from the presence of the reservoir. After we apply synthetic aperture to the 2D source, the average detectability ratio becomes 1.19. When the 2D synthetic aperture source is steered with the parameters found by the optimization, the average detectability ratio becomes 2.06. This corresponds to a 100% anomaly from the reservoir. From combining and steering sources from parts of three towlines, we increased the detectability of the reservoir from a small indication of its presence to a level where its existence is certain. The maximum of the average ratio between the inline electrical component with and without the reservoir is not the only choice for a measure of the improvement

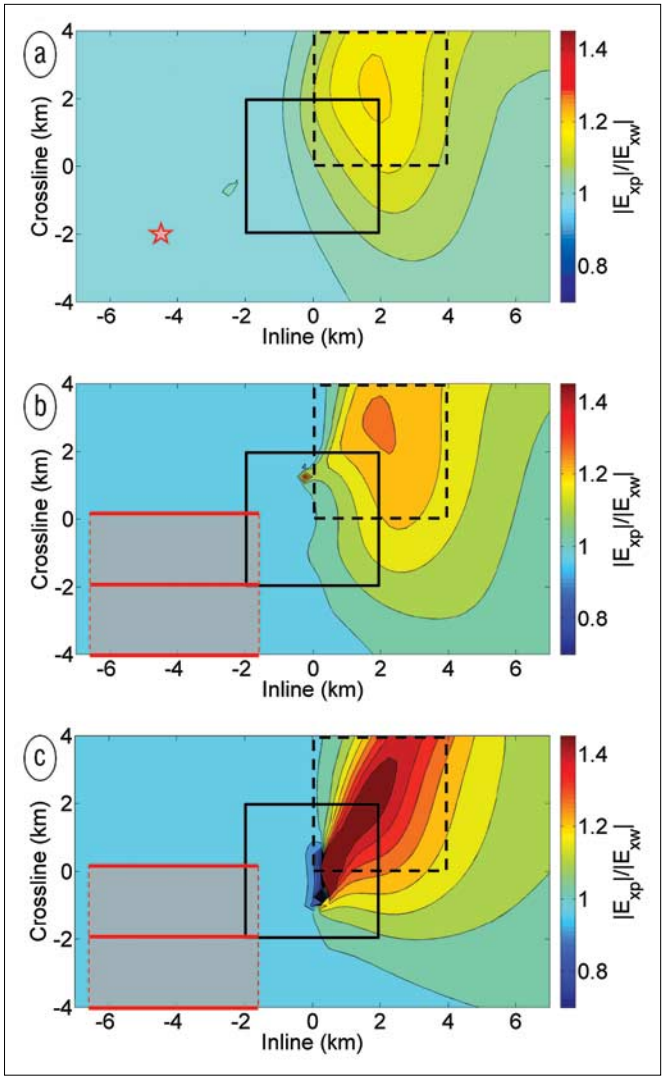

Figure 3. *The ratio of the absolute value of the inline electric component for a single source (a), a 2D synthetic aperture source (b), and a steered 2D synthetic aperture source (c). All three images depict the response at receivers on the ocean floor. The footprint of the reservoir is outlined in black and the source is outlined in red. The area of the expected reservoir anomaly is shown as the dashed black box.*

obtained with steering. Future research will focus on developing a more robust optimization scheme, possibly including more parameters such as number of sources and placement of sources. Maximizing the average ratio of the inline electric component with and without the reservoir demonstrates the increases in detectability that synthetic aperture can achieve.

Visualizing steered fields in 3D

To visualize the impact the steering has on the direction of the energy transport, we use the Poynting vector. The most common way to visualize electric and magnetic fields is through magnitude and phase plots, but these lack the capability to show the direction in which the field is propagating (Constable, 2010). The Poynting vector measures the direction in which the energy flux of the electromagnetic field is traveling; it is an effective way to examine how an electromagnetic field propagates (Fan et al., 2012). The energy flux

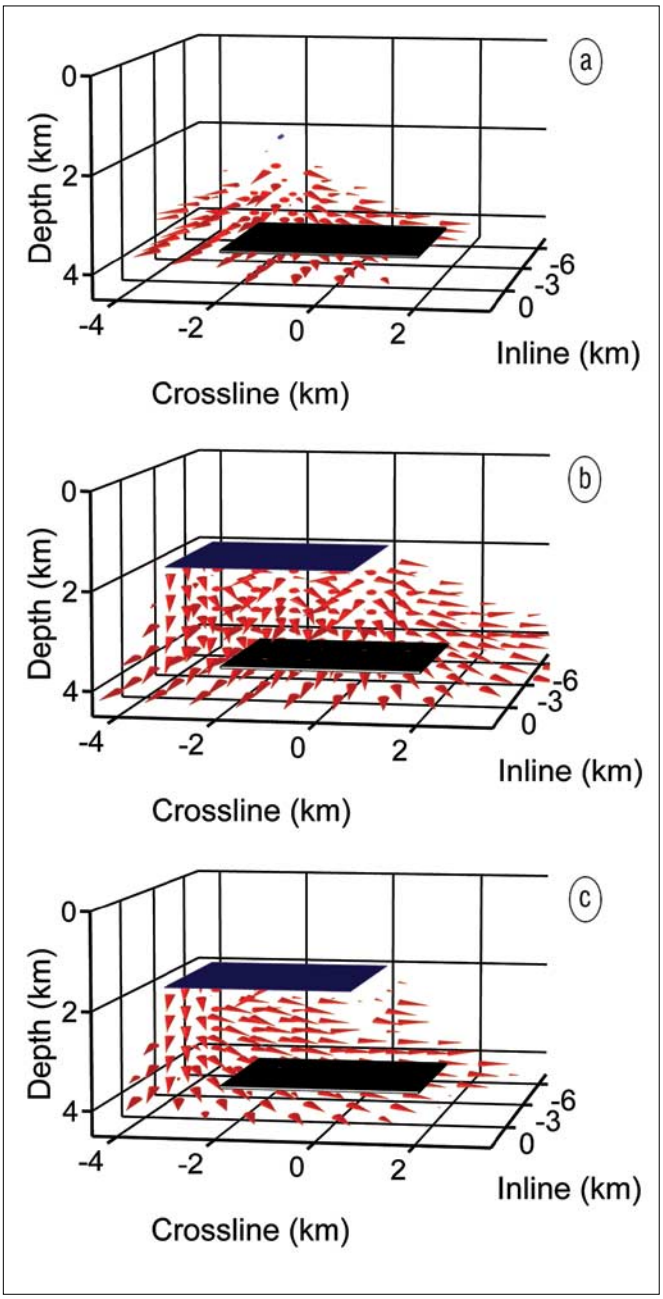

Figure 4. *The normalized, time-averaged Poynting vectors with z-component greater than zero for a single source (a), a 2D synthetic aperture source (b), and a steered 2D synthetic aperture source (c). The Poynting vectors from the 2-km water layer (including the air wave) have been removed for clarity. All three images depict the footprint of the reservoir in black and the source in blue.*

density of the electromagnetic field is given by

$$\mathbf{P} = \mathbf{E} \times \mathbf{H} \tag{5}$$

where **E** is the electric field and **H** is the magnetic field (Jackson, 1999). For frequency-domain fields, the Poynting vectors must be averaged over time to eliminate the oscillation of the source. The time-averaged Poynting vector is given by (Jackson, 1999)

$$\bar{\mathbf{P}} = 1/2\mathrm{Re}(\mathbf{E} \times \mathbf{H}^*) \tag{6}$$

The synthetic CSEM data set in this article is sampled in three dimensions which enables the Poynting vector of the field to be viewed in 3D as well. The resulting Poynting vector field is too dense to view all vectors at once. It is more demonstrative to show the downward-propagating field from the source. Figure 4 shows the Poynting vectors with z-component greater than zero for a single source, the 2D synthetic aperture source, and the steered 2D synthetic aperture source. The Poynting vectors from the 2-km water layer, which includes the air wave, are not shown to make the subsurface interactions of the field visible. The message of Figure 4 is the difference in direction of the Poynting vectors from the steered source when compared to the other sources. The steered source shifts the energy toward the reservoir in the crossline direction (Figure 4c) while the energy of the single source (Figure 4a) and unsteered 2D synthetic aperture source (Figure 4b) radiate downward and away from the reservoir. Our ability to steer in the crossline direction, shown in Figure 3c, is promising because even though the towlines are sparsely spaced, 2 km apart in the crossline direction, we are still able to achieve coherent steering of the energy with just three towlines. The Poynting vectors show an organization in the crossline direction that is not present in the vectors of the other sources. These vectors may assist in refining the optimization by defining the change in the direction of the energy propagating through the reservoir. The Poynting vector is a useful tool to view all parts of the electromagnetic energy propagating through the Earth.

Conclusion

The synthetic aperture technique offers a way to address some of the limitations of CSEM without requiring any changes in acquisition. Applying the technique to synthetic CSEM data demonstrates the possible increase to the detectability of hydrocarbon reservoirs. Steering the fields in both the inline and crossline directions sends more energy toward the reservoir rather than propagating out symmetrically. The implementation of these techniques increases the amount of information gleaned from data acquired from the CSEM survey, making CSEM a more valuable tool for industry. The application of synthetic aperture to real data follows the same process as the synthetic examples shown but it may be restricted by the acquisition geometry of the survey and quality of the data. We expect the technique to improve detectability in data with typical noise levels because of the summation of responses from several different sources. Research is ongoing to optimize the synthetic aperture source and to investigate the implications of synthetic aperture to the design of CSEM surveys. TLE

References

Barber, B. C., 1985, Review article. Theory of digital imaging from orbital synthetic-aperture radar: International Journal of Remote Sensing, **6**, no. 7, 1009–1057, http://dx.doi.org/10.1080/01431168508948262.

Bellettini, A. and M. A. Pinto, 2002, Theoretical accuracy of synthetic aperture sonar micronavigation using a displaced phase-center antenna: IEEE Journal of Oceanic Engineering, **27**, no. 4, 780–789, http://dx.doi.org/10.1109/JOE.2002.805096.

Constable, S., 2010, Ten years of marine CSEM for hydrocarbon exploration: Geophysics, **75**, no. 5, A67–A81, http://dx.doi.org/10.1190/1.3483451.

Constable, S. and L. J. Srnka, 2007, An introduction to marine controlled-source electromagnetic methods for hydrocarbon exploration: Geophysics, **72**, no. 2, WA3–WA12, http://dx.doi.org/10.1190/1.2432483.

Edwards, N., 2005, Marine controlled source electromagnetics: Principles, methodologies, future commercial applications: Surveys in Geophysics, **26**, no. 6, 675–700, http://dx.doi.org/10.1007/s10712-005-1830-3.

Fan, Y., R. Snieder, E. Slob, J. Hunziker, and J. Singer, 2011, Steering and focusing diffusive fields using synthetic aperture: Europhysics Letters, **95**, no. 3, 34006, http://dx.doi.org/10.1209/0295-5075/95/34006.

Fan, Y., R. Snieder, E. Slob, J. Hunziker, J. Singer, J. Sheiman, and M. Rosenquist, 2010, Synthetic aperture controlled-source electromagnetics: Geophysical Research Letters, **37**, no. 13, L13305, http://dx.doi.org/10.1029/2010GL043981.

Fan, Y., R. Snieder, E. Slob, J. Hunziker, J. Singer, J. Sheiman, and M. Rosenquist, 2012, Increasing the sensitivity of controlled-source electromagnetics with synthetic aperture: Geophysics, **77**, no. 2, E135–E145, http://dx.doi.org/10.1190/geo2011-0102.1.

Hursán, G. and M. Zhdanov, 2002. INTEM3D. http://www.cemi.utah.edu/soft/index.html.

Jackson, J. D., 1999, Classical electrodynamics: Wiley.

Jensen, J. A., S. I. Nikolov, K. L. Gammelmark, and M. H. Pedersen, 2006, Synthetic aperture ultrasound imaging: Ultrasonics, **44**, Suppl 1, e5–e15, http://dx.doi.org/10.1016/j.ultras.2006.07.017.

Løseth, L., M. H. Pedersen, B. Ursin, L. Amundsen, and S. Ellingsrud, 2006, Low-frequency electromagnetic fields in applied geophysics: Waves or diffusion?: Geophysics, **71**, no. 4, W29–W40, http://dx.doi.org/10.1190/1.2208275.

Mandelis, A., 2000, Diffusion waves and their uses: Physics Today, **53**, no. 8, 29–34, http://dx.doi.org/10.1063/1.1310118.

Van Veen, B. and K. Buckley, 1988, Beamforming: a versatile approach to spatial filtering: IEEE ASSP Magazine, **5**, no. 2, 4–24, http://dx.doi.org/10.1109/53.665.

Wang, C. and A. Mandelis, 1999, Purely thermal-wave photopyroelectric interferometry: Journal of Applied Physics, **85**, no. 12, 8366–8377, http://dx.doi.org/10.1063/1.370684.

Yodh, A. and B. Chance, 1995, Spectroscopy and imaging with diffusing light: Physics Today, **48**, no. 3, 34–40, http://dx.doi.org/10.1063/1.881445.

Acknowledgments: We are grateful for the financial support from the Shell Gamechanger Program of Shell Research, and thank Shell Research for the permission to publish this work.

Corresponding author: aknaak@mines.edu